

# *iGCI*: An Integrated Fluidic System for Gas Chromatography Including Knudsen Pump, Preconcentrator, Column, and Detector Microfabricated by a Three-Mask Process

Yutao Qin and Yogesh B. Gianchandani, *Fellow, IEEE*

**Abstract**—This paper reports an integrated microscale gas chromatography ( $\mu$ GC) system, the *iGCI*, which contains four components: 1) a Knudsen pump (KP); 2) a preconcentrator-focuser (PCF); 3) a separation column; and 4) a gas detector. All four components are fabricated from glass wafers using a three-mask process with minimal postprocessing. In a stackable architecture, the components are finally assembled into a 4-cm<sup>3</sup> system. The stacked *iGCI* system demonstrates the successful separation and detection of an alkane mixture in the range of C<sub>5</sub>–C<sub>8</sub> in less than 60 s. [2013-0230]

**Index Terms**—Nanoporous, thermal transpiration, microdischarge, emission spectrum, gas sensors.

## I. INTRODUCTION

A GAS CHROMATOGRAPH (GC) is an instrument used to spatiotemporally separate and detect vapors by passing sample plugs through a channel (*i.e.*, the column) coated with a functional material (*i.e.*, the stationary phase). The constituents can be identified by the time taken to elute from the column and quantified by the strength of the signal from a detector located downstream of the column. In general, many other components are also integral to the operation, such as the preconcentrator that provides sample injection, and the pump that generates the flow. In some systems valves are used to control the timing and direction of the flow. The separation of complex mixtures is sometimes performed using comprehensive two-dimensional GC (2DGC or GC  $\times$  GC).

Since the widespread adoption of the GC by the petroleum industry in the 1950s, its use has been extended to a number of other fields. For example, it is used to examine pollutants, such as polycyclic aromatic hydrocarbons, pesticides, halogenated compounds, *etc.* [1]. Another application is food analysis: coupled with the solid-phase microextraction technique, it is used for the identification and quantification of lipids, drugs,

pesticides and carbohydrates [2]. In recent years biomedical screening has also been performed by this instrument. The analysis of human exhaled biomarkers by the GC provides a non-invasive approach for diagnosis and monitoring of potential diseases. Examples of such biomarkers include nitric oxide related to pulmonary inflammation, and ethane and pentane related to lipid peroxidation [3].

The miniaturization of the GC has been an ongoing effort for over 30 years, with early work dating back to 1979, when Terry *et al.* reported a silicon micromachined GC system [4]. As the core component of a micro gas chromatography ( $\mu$ GC) system, the separation column has been widely investigated and various column structures have been reported, such as the nickel column [5], the silicon-glass column [6], the Parylene<sup>TM</sup> column [7] and the plasma-enhanced chemical vapor deposition (PECVD) oxynitride column [8]. The stationary phase coating methods for these columns include the static coating method [9] as well as the dynamic coating method [10]. A self-assembly process has also been reported [11]. The gas injection device for a  $\mu$ GC system can be mainly classified into two categories: the preconcentrator and the valve injector. The preconcentrator uses sorbents to collect analytes at low temperatures and inject a plug with a thermal pulse [12]–[14]. Certain preconcentrators collect analytes without the need for gas flow [15]. Conversely, the valve injector utilizes valves to sample and inject a plug of gas [16]. A variety of gas detectors have been reported, including the chemiresistor [17], the chemicapacitor [18], the thermal conductivity detector [19], the Fabry-Pérot detector [20], and the discharge-based detector [21], [22]. A microfabricated thermal modulator has been reported [23] and its application in a GC  $\times$  GC has also been reported [24].

The integration of the microfabricated components into a  $\mu$ GC system has also made remarkable progress. The  $\mu$ ChemLab [25] is a hand-held  $\mu$ GC system reported by Lewis *et al.* that consists of a preconcentrator, a column, and surface acoustic wave sensors. Researchers at the University of Michigan have reported several prototypes of  $\mu$ GC over the past decade, including the Intrepid [26], the Spiron [27] and the palm-size Mercury system [28].

Most  $\mu$ GC research efforts have not incorporated the use of micropumps. Only two cases have been reported: one with a microfabricated, electrostatically-actuated peristaltic

Manuscript received July 20, 2013; revised October 19, 2013; accepted January 29, 2014. Date of publication March 4, 2014; date of current version July 29, 2014. This work was supported in part by the Microsystems Technology Office, Defense Advanced Research Projects Agency High-Vacuum Program, under Contract W31P4Q-09-1-0011, and in part by the Lurie Nanofabrication Facility through the Solid-State Electronics Laboratory and the University of Michigan, Ann Arbor, MI, USA. Subject Editor C. Ahn.

The authors are with the Center for Wireless Integrated MicroSensing and Systems, University of Michigan, Ann Arbor, MI 48109 USA (e-mail: yutaoqin@umich.edu; yogesh@umich.edu).

Color versions of one or more of the figures in this paper are available online at <http://ieeexplore.ieee.org>.

Digital Object Identifier 10.1109/JMEMS.2014.2306652

pump [29], and another with an array of motionless Knudsen pumps [30]. The former required high frequency, large amplitude, drive voltages, but was power-efficient. The latter was not power-efficient, but required only a low-voltage DC source; it provided high reliability, with continuous operation for over 6000 hours [31].

Many micropump-operated  $\mu$ GC systems reported to date have used components fabricated by disparate microfabrication processes. Some systems connect the components by tubing (*e.g.*, [26]–[30]), whereas some use manifolds for fluidic interconnect (*e.g.*, [32]–[35]). The benefit of this approach is that each component can be optimally designed and fabricated. Unfortunately, the increased complexity and cost of the fabrication of the whole system pose a challenge for integration. As in other fluidic systems, a stackable architecture (*e.g.*, [36]) or a monolithic integration scheme (*e.g.*, [37]) can alleviate this problem. Additionally, using a simple and easily available microfabrication process for all of the components would greatly benefit the manufacturability and integration of the system.

This paper reports the use of a simple 3-mask fabrication process for simultaneously manufacturing a preconcentrator, a separation column, a discharge-based detector, and a Knudsen pump. Design innovations at the device level are used to accommodate this facile process, followed by system assembly.<sup>1</sup> A stackable architecture is used for the system integration scheme, eliminating the use of tubing for gas flow interconnects and providing a path for further miniaturization.

As opposed to the pump array [30] that included six KPs fabricated by drill machining, the *iGCI* system uses a single KP that is for the first time designed for integration within a  $\mu$ GC and micromachined lithographically. It also provides at least an order of magnitude improvement in footprint and power.

The design and modeling of the *iGCI* system are described in Section II, the fabrication process is described in Section III, experimental results are presented in Section IV, followed by the discussion and conclusions in Section V.

## II. DESIGN AND MODELING

### A. Knudsen Pump

Knudsen pumps are driven by thermal transpiration in narrow channels that constrain flow to the free-molecular or transition flow regimes. Gas molecules move against a temperature gradient, *i.e.*, from the cold end to the hot end of the channels; the pump itself has no moving parts. In this effort, the Knudsen pump (Fig. 1) consists of three glass dice (Die 1–3, thickness = 500  $\mu$ m) sandwiching a stack of nanoporous mixed cellulose ester (MCE) membranes (thickness  $\approx$  105  $\mu$ m, pore diameter  $\approx$  25 nm, porosity  $\approx$  70%, Millipore, MA). The membranes are cut to  $1.2 \times 1.2$  cm<sup>2</sup> squares, which form the active pumping areas. The pore diameter is on the same order of magnitude as the mean free path of air near atmospheric pressure. Multiple grooves on Die 1 and multiple through-holes on Die 2 facilitate the gas

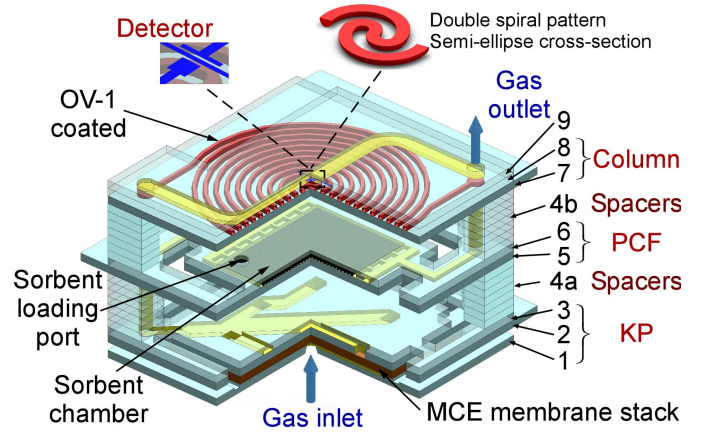


Fig. 1. Structural concept of the *iGCI* system.

flow through the MCE membrane, while the grooves on Die 3 guide the gas flow into the upper components. The temperature gradient is applied by a thin-film heater on Die 2 and an external heat sink attached to the bottom of Die 1. In this work the heat sink is a simple aluminum plate with a perforation at the gas inlet. Its footprint is slightly larger than the Knudsen pump.

Because of its computational ease and relative accuracy, Sharipov's model is often used for estimating the thermal transpiration phenomenon in microfabricated Knudsen pumps, which typically have long and convoluted channels [31], [39]. The thermal transpiration driven mass flow in a channel of circular cross section is provided by:

$$M_{avg} = \left[ Q_T \frac{\Delta T_{KP}}{T_{avg}} - Q_P \frac{\Delta P_{KP}}{P_{avg}} \right] \frac{\pi a^3 P_{avg}}{l} \left[ \frac{m}{2k_B T_{avg}} \right]^{\frac{1}{2}} \quad (1)$$

where  $\Delta T_{KP}$ ,  $\Delta P_{KP}$ ,  $T_{avg}$  and  $P_{avg}$  are the temperature difference, pressure difference, average temperature and average pressure between the hot end and the cold end of the channel, respectively,  $a$  is the channel radius,  $l$  is the channel length,  $m$  is the mass of the gas molecule, and  $k_B$  is the Boltzmann constant. The parameters  $Q_T$  and  $Q_P$  are, respectively, the temperature and pressure flow coefficients, which were tabulated by Sharipov [39]. The values of these coefficients depend on the rarefaction parameter,  $\delta_{avg}$ , which is given by:

$$\delta_{avg} = \frac{\sqrt{\pi} a}{2 \lambda_{avg}} \quad (2)$$

where  $\lambda_{avg}$  is the mean free path of the gas molecule.

The volumetric flow rate of a Knudsen pump with numerous parallel channels can be calculated as:

$$Q_{KP} = \frac{M_{avg} \cdot N_{channel}}{\rho_{gas}} \quad (3)$$

where  $N_{channel}$  is the total number of channels for thermal transpiration and  $\rho_{gas}$  is the density of the gas.

Based on equations (1)–(3), the Knudsen pump described for this effort is estimated to provide 6.7 sccm unloaded air flow rate with  $\Delta T_{KP} = 60$  °C. Its blocking pressure, the maximum  $\Delta P_{KP}$ , is estimated to be 6.7 kPa [by letting  $M_{avg} = 0$  in equation (1)].

<sup>1</sup>Portions of this paper have appeared in conference abstract form in [38].

### B. Preconcentrator

The preconcentrator adsorbs the analyte molecules onto a porous surface at room temperature. To initiate analysis, sample is desorbed with a thermal pulse and injected into the fluidic path. This work utilizes a single bed preconcentrator, designed as an 11 mm<sup>3</sup> chamber formed by Die 5 and Die 6 (Fig. 1). Granules of Carbograph<sup>TM</sup> 2 (Grace Davison Discovery Sciences, IL), a graphitized carbon with a surface area of 10 m<sup>2</sup>/g, are packed in the chamber as the sorbent material. In addition to the gas inlet and outlet features, the preconcentrator contains a sorbent loading port from which the sorbent granules can be loaded. The arrays of pillars are designed to confine the sorbent granules in the chamber.

The theoretical modeling of the sorbent-packed preconcentrators is often described using the Wheeler-Jonas model [40]. The breakthrough time  $t_b$  (min.) is a metric for characterizing the adsorption capability. Specifically, it is the time required for vapor that enters the preconcentrator to saturate and reach a certain concentration at outlet (expressed as a fraction of that at inlet):

$$t_b = \frac{W_e}{Q \cdot c_{in}} \left[ W - \frac{Q \cdot \rho_b}{k_v} \ln \left( \frac{c_{in}}{c_{out}} \right) \right] \quad (4)$$

where  $W_e$  is the adsorption capacity that can be theoretically derived [40],  $W$  is the total sorbent mass (g),  $Q$  is the volumetric flow rate (cm<sup>3</sup>/min.),  $c_{in}$  is the inlet chemical concentration (g/cm<sup>3</sup>),  $\rho_b$  is the bulk density of the packed sorbent (g/cm<sup>3</sup>),  $k_v$  is the overall mass transfer coefficient (min.<sup>-1</sup>) that can be estimated from semi-empirical equations [41], and  $c_{out}$  is the outlet chemical concentration chosen to denote breakthrough (g/cm<sup>3</sup>).

The preconcentrator is designed to have the largest achievable sorbent chamber without compromising the thermal isolation and form factor of the system (Fig. 1). As described in Section IV,  $t_b$  is experimentally measured by setting  $c_{in} = 80$  ppm (determined by mole fraction of the sample vapor in the carrier gas used in this effort) and  $Q = 1$  sccm, while using a breakthrough criterion  $c_{out}/c_{in} = 10\%$ .

### C. Column

The column separates analyte species as they pass along, based on the partition that each analyte establishes between the mobile phase (carrier gas) and the stationary phase. In this effort, the column is designed as a channel (length  $\approx 25$  cm) laid out in a double-spiral pattern and formed by the bonding of Die 7 and Die 8 (Fig. 1). The manufacturing process creates an approximately semi-elliptical cross section (width  $\approx 300$   $\mu$ m, depth  $\approx 200$   $\mu$ m), which has a hydraulic diameter  $\approx 230$   $\mu$ m (defined as  $4 \times \text{area/perimeter}$ ). A  $\approx 0.2$   $\mu$ m thick non-polar polydimethylsiloxane (OV-1, Ohio Valley Specialty, OH) layer is coated on the inner walls as the stationary phase.

The separation efficiency of a chromatography column can be evaluated from experimentally obtained chromatograms. Higher separation efficiency is denoted by higher number of plates,  $N$ , as well as smaller dimension of a theoretical plate, termed the ‘‘height equivalent to a theoretical plate (HETP).’’

The HETP can be theoretically estimated from the structural dimensions and physical properties of the column, although these are not always well known [42]. The HETP of the column can be calculated accordingly, which facilitates the evaluation and comparison of columns with various lengths.

$$N = 5.54 \left( \frac{t_R}{W_{1/2}} \right)^2 \quad (5)$$

$$\text{HETP} = \frac{l_{column}}{N} \quad (6)$$

where  $t_R$  is the retention time,  $W_{1/2}$  is the width of the retention peak measured at half height, and  $l_{column}$  is the length of the separation column. For this work,  $l_{column}$  is  $\approx 25$  cm. The experimentally-determined values of  $t_R$  and  $W_{1/2}$  are described in Section IV, along with the resulting HETP.

### D. Detector

The discharge-based gas detector uses two metal electrodes to create localized microdischarges, which generate optical spectra indicating the presence of carbon atoms. Although RF-powered microdischarges and DC microdischarges are options as summarized in [43], pulsed DC microdischarges are used because they consume low power, require a simple interface circuit, and offer an extended lifetime [43], [44]. As shown in Fig. 1, the electrodes for creating microdischarges, spaced 50  $\mu$ m apart, are located on Die 8, while the groove structure of Die 9 guides the gas to pass over the detector. The optical signal is detected by a hand-held spectrometer (Model # USB 2000, Ocean Optics, FL), which is controlled by a laptop computer.

### E. Stacked iGCI Assembly

The four components are arranged in a stack, forming a serially connected gas flow path (Fig. 1). Driven by the Knudsen pump located upstream, the preconcentrator accumulates analytes and desorbs them along the same gas flow direction. The desorbed gas analytes pass through the column with characteristic retention times that are temporally resolved by the detector. Thermal crosstalk between the pump, preconcentrator, and separation column is inhibited by glass spacers (Dice 4a and Dice 4b) and the cut-outs (voids) in each layer. Depending on the system requirements, more spacers can be added to the system to achieve superior thermal isolation.

### F. Thermal Modeling of the Stacked iGCI Assembly

The thermal behavior of the stacked iGCI assembly was modeled using finite element analysis (FEA) in COMSOL Multiphysics 4.2. The simulations were directed at modeling the temperature distributions of the system while the Knudsen pump or the preconcentrator is heated. In both cases, the simulated structure included 7 spacers both between the preconcentrator and the column as well as between the preconcentrator and the Knudsen pump, mimicking the actual system used for experimental tests. The thermal conductance of the MCE membrane stack in the Knudsen pump was derived from an experimentally fitted equivalent value. The bottom of

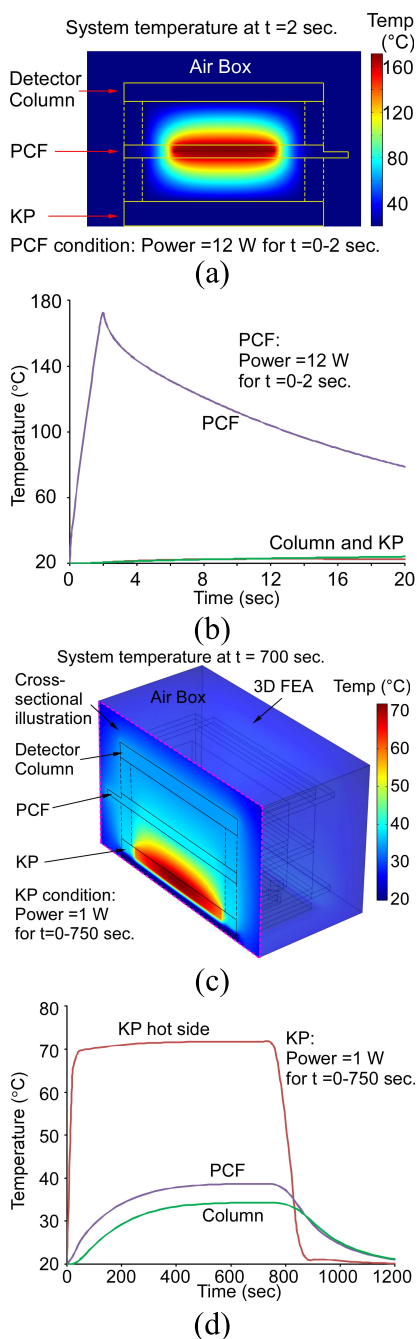


Fig. 2. The FEA simulation result of the thermal response of the *iGCI* system. (a) The temperature profile of the system after heating the preconcentrator with 12 W for 2 sec. (b) The transient thermal response of the system during a thermal cycle of the preconcentrator. (c) The temperature profile of the system after heating the Knudsen pump with 1 W for 700 sec. (d) The transient thermal response of the system during a thermal cycle of the Knudsen pump.

the Knudsen pump was assumed to be maintained at room temperature by an ideal heat sink. The system was surrounded by an air box with natural convective heat transfer to the ambient.

In the case where the preconcentrator is heated, it is subject to a thermal pulse (12 W, 2 sec.) and reaches 170 °C [Fig. 2(a) and (b)]. Because of the thermal isolation offered by the spacers and the pulsed nature of the heating, the column and the Knudsen pump are only minimally affected.

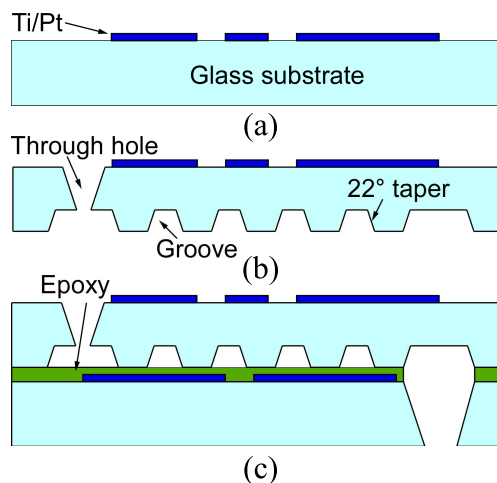


Fig. 3. (a) Deposition and patterning of a Ti/Pt metal layer on a glass wafer. (b) Two-step sandblasting to create the groove structures and through-wafer vias and cutouts. (c) Epoxy bonding of two glass dice.

In the case where the Knudsen pump is actuated, there is a 50 °C temperature difference across the MCE membrane stack with 1 W input power [Fig. 2(c) and (d)]. The simulation shows that the maximum parasitic temperature rises, after reaching steady state in  $\approx 400$  sec., are  $\approx 18$  °C in the preconcentrator and  $\approx 14$  °C in the separation column. This thermal crosstalk, which exists during both vapor sampling and analytical separation, is small enough that the preconcentrator and the column remain functional. The exact thermal crosstalk depends on how the system is operated. For vapor sampling and separation times shorter than 400 sec., the thermal crosstalk is smaller.

### III. FABRICATION PROCESS

The fabrication process can be divided into two major steps. The first is the lithographic microfabrication: a common 3-mask sequence is used for all the four *iGCI* components. The second is the assembly of the system.

#### A. Lithographic Process

The lithographic microfabrication utilizes one mask for metallization and two masks for micromachining. Borosilicate glass is selected as the substrate material in this effort. However, any other kind of glass, including the low-cost sodalime glass can be used. To start with, a metal layer (Ti/Pt 25/100 nm) is deposited by e-beam evaporation and patterned by liftoff on a 500  $\mu\text{m}$  thick glass wafer [Fig. 3(a)], forming heaters, temperature sensors and microdischarge electrodes. The metallized wafer is subject to a two-step machining process that grooves the non-metallized side of the wafer and creates through-wafer vias and cutouts [Fig. 3(b)]. Each of the micromachining steps requires a mask. In this effort, a micro abrasive jet machining (sandblasting) was used (Bullen Ultrasonics, OH). The grooved structures form in-plane gas flow paths; the through-wafer vias form the inter-layer gas flow paths; and the through-wafer cutouts provide in-plane thermal isolation and stackable spacers. The sandblasted features typically have a 22° taper angle and a corner radius of 125  $\mu\text{m}$ . The depth and feature sizes of the groove structures

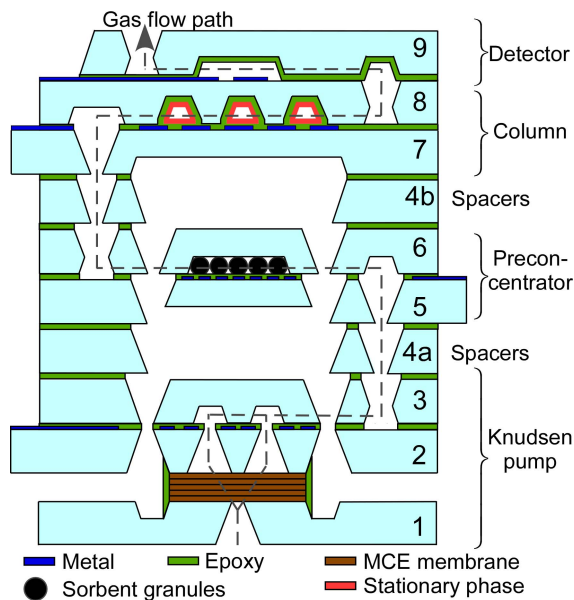


Fig. 4. The illustrated cross section of the *iGCI* system after the final stacking.

are in the range of 150–300  $\mu\text{m}$ . In addition to sandblasting, many other approaches are available for micromachining glass wafers, such as plasma etching, wet etching and ultrasonic machining.

### B. Assembly Process

If each component is fabricated on a separate wafer, system assembly can be performed at the wafer level. In this work, however, all the components are on the same wafer, so the dice are singulated prior to assembly. Each of the components is then epoxy bonded to its upper layer [Fig. 3(c)] before being added to the system stack (Fig. 4).

The Knudsen pump is assembled into a glass-MCE-glass stack. Die 2 and Die 3 are first bonded by a low-viscosity epoxy Epotek 377 (Epoxy Technology, MA), which is applied from the perimeter of the dice that are arranged in a stack, and drawn into the seams between the mating surfaces by capillary force. Curing at 150  $^{\circ}\text{C}$  forms a leak free bond between the two glass dice. Next, Die 2, Die 3, four MCE membranes, and Die 1 are stacked (in order from top to bottom as stated). Finally, a viscous epoxy Stycast2850FT (Henkel, Düsseldorf, Germany) is applied around the edge of the MCE membrane stack to achieve a hermetic seal, which is crucial to the operation of the Knudsen pump.

The preconcentrator is assembled by epoxy bonding and sorbent packing. Die 5 and Die 6 are bonded by Epotek 377. Next, sorbent granules are packed into the preconcentrator using a similar method to that described in [15]. Moderate vacuum from the inlet/outlet is used to draw the Carboxgraph 2 granules from the loading port into the preconcentrator. The pillar structures in the preconcentrator act as sieves to contain larger particles while letting smaller particles to pass through and exit the preconcentrator. After sorbent loading, the loading port is sealed with either thermal tape or epoxy.

The separation column is assembled by a coated layer of SU-8 5 (MicroChem, MA). Omnicast (MicroChem, MA) is spin-coated and baked as the adhesion promoter, followed by a layer (less than 10  $\mu\text{m}$ ) of SU-8 spin-coated on the mating surfaces – specifically, the metallized side of Die 7 and the grooved side of Die 8. The grooved die (Die 8) is softbaked at 150  $^{\circ}\text{C}$  in order to prevent the potential problem of fluid SU-8 filling and blocking the channel. Then the dice are aligned and stacked, followed by a second softbake at 95  $^{\circ}\text{C}$ , which drives the fluid SU-8 to gradually fill the gaps and voids between the mating surfaces, providing a leak free bond. The device is exposed to ultraviolet (UV) radiation and hardbaked at 150  $^{\circ}\text{C}$  to cure the SU-8 and minimize outgassing. The spin-coating process described above fully covers the inner walls of the separation column with SU-8, providing two potential benefits for obtaining a more uniform coating of stationary phase. First, the inner surface of the column is a homogeneous material that provides uniform adhesion strength to the stationary phase. Second, any surface roughness on the grooves that may result from the sandblasting is smoothed by the SU-8 layer.

The SU-8 bonded column is then coated with a  $\approx 0.2$   $\mu\text{m}$  thick layer of OV-1 stationary phase using a conventional static coating method [9]. In this process, a solution of OV-1 is prepared by dissolving OV-1 and its cross-linking agent dicumyl peroxide in pentane and filled into the column. With one end of the column sealed, pentane is evaporated from the other end of the column by vacuum, leaving OV-1 coated on the inner walls of the column. After that, the column is heated at 150  $^{\circ}\text{C}$  overnight to fully remove the solvent as well as to perform cross-linking. This coating process can be assisted by capillary tubes temporarily attached to both ends of the column using the epoxy Stycast2850FT; the capillary connections can be easily detached by localized heat after the coating process.

The detector is assembled by bonding Die 9 to Die 8 with Epotek 377 using the process as described for assembling the Knudsen pump.

The overall system is finally integrated by the assembly of all four components together with a number of spacers (Fig. 4), which are micromachined by sandblasting on the same glass wafer as the other dice. The spacers can be permanently bonded to the *iGCI* components using Epotek 377. However, a removable bonding layer between the components is also favored to allow reconfigurability. With low melting points and easy solubility in common solvents, various kinds of mounting wax have been widely used as temporary adhesives in the industry. The mounting wax QuickStick<sup>TM</sup> 135 (Electron Microscopy Sciences, PA) is used in this effort to provide the removable bonding layers. When assembling the system, the components are placed on a hot plate at 150  $^{\circ}\text{C}$ . The mounting wax is melted by the elevated temperature and applied to the mating surfaces. The components are then pressed together, allowing the mounting wax to form a leak free bond. The thermal operation of the *iGCI* system does not damage this bond as long as no strong shear force is applied. When it is necessary to reconfigure the *iGCI* system, the stack can be heated on a hot plate and the bond can be easily detached.

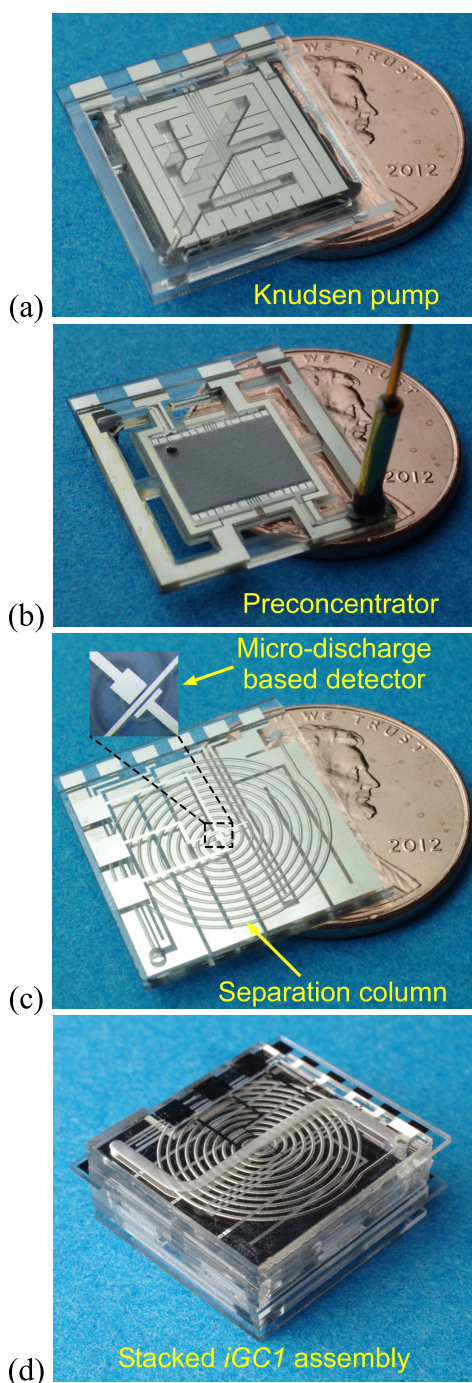


Fig. 5. The machining and assembly of the *iGCI* system. Photographic images of (a) the Knudsen pump, (b) the preconcentrator, (c) the separation column and the discharge-based detector, and (d) the *iGCI* stack assembly.

The bottom surface of the *iGCI* stack can be attached to an aluminum plate, which serves as a heat sink for the Knudsen pump. Capillary tubes can be attached to the inlet and outlet of the *iGCI* system for testing.

Figure 5 shows fabrication results of various elements. The *iGCI* system has a footprint of  $3.2 \text{ cm}^2$  and a height dependent on the number of spacers in the stack; a typical system tested in this effort has 14 spacers in total, corresponding to a total height of  $\approx 1.15 \text{ cm}$  and a form factor of  $3.7 \text{ cm}^3$ .

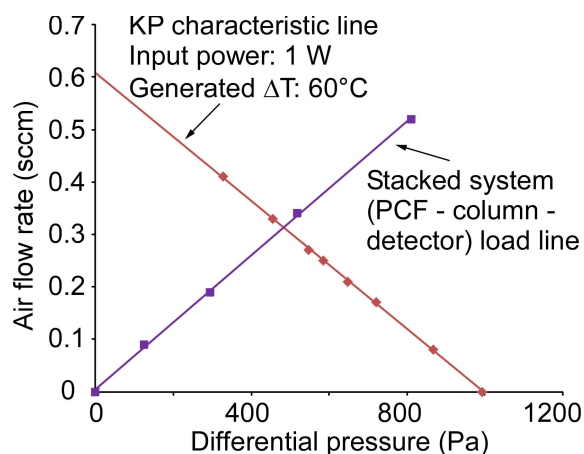


Fig. 6. The steady state performance of the Knudsen pump and the gas flow load of the system tested in room air.

#### IV. EXPERIMENTAL RESULTS

Prior to the assembly of the full *iGCI* system, each component was separately evaluated. The experimental evaluations focused on alkanes in the range of  $C_5$ – $C_8$  for simplicity and benchmarking purposes. These alkanes are also indicative of the system response to typical indoor pollutants. The results are presented below.

##### A. Pump and Gas Flow

In the evaluation of the Knudsen pump, its inlet was exposed to the ambient at atmospheric pressure, while varying loads (manifested as capillary tubes with varying length) were connected to its outlet. The values of the loads were selected to span over a wide range covering the actual load provided by the system. A commercial pressure sensor (Model # MPX5010DP, Freescale Semiconductor, AZ) and a flow meter (Part # FMA-1603A, Omega Engineering, CT) were connected between the outlet and the capillaries to monitor the pressure and flow conditions, respectively. With 1 W input power, the pump generated a  $\Delta T_{KP}$  of  $\approx 60^\circ\text{C}$ , and was able to provide a steady state flow rate of 0.41 sccm against a pressure of 330 Pa; it provided a maximum pressure of 1 kPa. The flow rate declines linearly with load pressure (Fig. 6). The deviation of experimental data from the theoretical estimates is likely due to imperfections in the MCE membranes or in the loss of a portion of the temperature gradient in the air gap between the heater and the membrane [31].

The load presented by the *iGCI* system was measured using a similar setup. The only differences were: an external pump replaced the Knudsen pump and the component stack (including preconcentrator, column, and detector) replaced the capillary tubes. With the data points linearly fitted into a load line, the flow conductance of the stacked preconcentrator, column and detector can be read from the slope  $-0.64 \text{ sccm/kPa}$  (Fig. 6). The system operating point is indicated by the intersection between the Knudsen pump curve and the system load line.

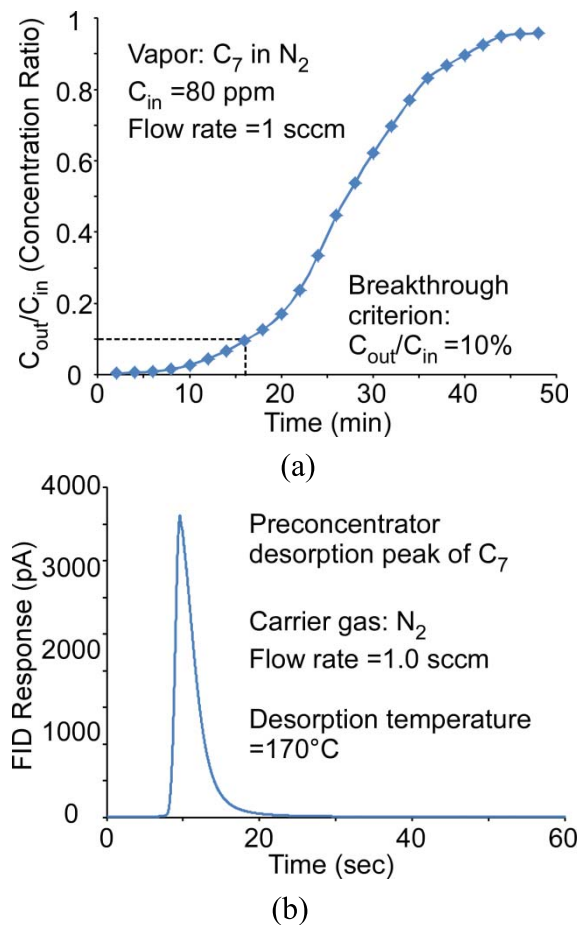


Fig. 7. The evaluation of the performance of the preconcentrator. (a) A sample breakthrough experiment by challenging the preconcentrator with heptane and measuring the vapor concentration at its outlet. (b) A heptane desorption peak provided by the preconcentrator with  $N_2$  carrier gas.

### B. Preconcentrator

The preconcentrator was characterized for both adsorption and desorption. The adsorption capability of the preconcentrator was experimentally evaluated by measuring the time taken by the vapor concentration at its outlet to reach a certain fraction of that at its inlet; this is known as “breakthrough.” In this effort, the inlet of the preconcentrator was connected to a 2 L dilution bottle (Sigma Aldrich, WI) containing 80 ppm heptane in  $N_2$ ; the vapor was drawn by a vacuum pump to pass through the preconcentrator at 1 sccm flow rate; the vapor concentration at the outlet was routed through a six-port valve to a flame ionization detector (FID) within a commercial Agilent 6890 GC. At two-minute intervals, the valve routed a fixed volume (100  $\mu$ L) of the vapor downstream of the preconcentrator into the FID.

In Fig. 7(a), the heptane concentration at the preconcentrator outlet is normalized to that at its inlet. The preconcentrator saturated after 45 minutes of sampling and the heptane concentration at its outlet approached the concentration at its inlet. Conventionally, the breakthrough criterion is defined to be the outlet concentration that is 10% of that at the inlet [13]. For this work, this value corresponds to a breakthrough time of 16 minutes and a breakthrough volume of 16 mL for heptane.

The thermal desorption of the preconcentrator was evaluated by the desorption peak in the chromatogram. The preconcentrator was first used to sample the heptane vapor and then connected to the Agilent 6890 GC where it was positioned upstream of the FID and downstream of the injection port. The desorption was performed by applying a pulse using the integrated thin-film heater, which heated the preconcentrator to 170 °C in 2 sec. The carrier gas was  $N_2$  at a flow rate of 1 sccm; flow direction in the preconcentrator was the same during both sampling and desorption. As shown in Fig. 7(b), a 1.4 sec. desorption peak (measured at half height of the peak) is observed from the FID chromatogram with only minimal tailing. A second thermal pulse did not provide any additional desorption peak, verifying full desorption during the first thermal pulse. This characterization of the preconcentrator is a representation of its general capability rather than its actual performance within the *iGCI* system. This is because the *iGCI* system is operated at a lower flow rate of  $\approx 0.2$  sccm. Not only is this more easily accommodated by the pump, but the performance of the separation column is better at this flow rate.

### C. Column

The separation column was evaluated by an Agilent 6890 GC system by positioning it downstream of an injection port and upstream of an FID. Sample chromatograms obtained with the tested column are shown in Fig. 8. At room temperature, three alkane species ( $C_5$ ,  $C_7$ , and  $C_8$ ) were separated by the column in about 52 sec. [Fig. 8(a)]. With a 30 sec.-long linear ramping of temperature from 25 °C to 75 °C provided by the on-chip heater, the column separated the same alkane mixture with the same gas flow rate in 30 sec. [Fig. 8(b)]. Both chromatograms were obtained using  $N_2$  as the carrier gas at 0.17 sccm flow rate.

Golay plots are curves indicating how the column efficiency is affected by the carrier gas flow rate, which are helpful in determining the optimal operating point of the column. In this effort, a Golay plot was obtained by testing the separation column at room temperature for a number of  $N_2$  carrier gas flow rates. The  $C_8$  peak was used for calculating the number of plates  $N$  and the height-equivalent-to-a-plate HETP based on equations (5) and (6). As shown in Fig. 8(c), the column has an optimal operating point at the gas velocity range of 5–10 cm/sec. (corresponding to the flow rate of 0.15–0.3 sccm), which gives HETP  $\approx 0.04$  cm and a plate number ( $1/\text{HETP}$ ) of  $\approx 2600$  plates/m. This performance is comparable to other microfabricated columns that have been previously reported – 2000 plates/m [10], 3000 plates/m [11], and 4200 plates/m [9].

### D. Detector

The detector uses pulsed discharges that are controlled by the circuit shown in Fig. 9(a). In this circuit, the discharge energy is provided by capacitor  $C$ , which is charged by a single 1000-V pulse through  $R1$ . Once the anode reaches the breakdown voltage, which is typically  $\approx 650$  V, the discharge is initiated. Resistors  $R2$  (the ballast resistor) and  $R3$  are used

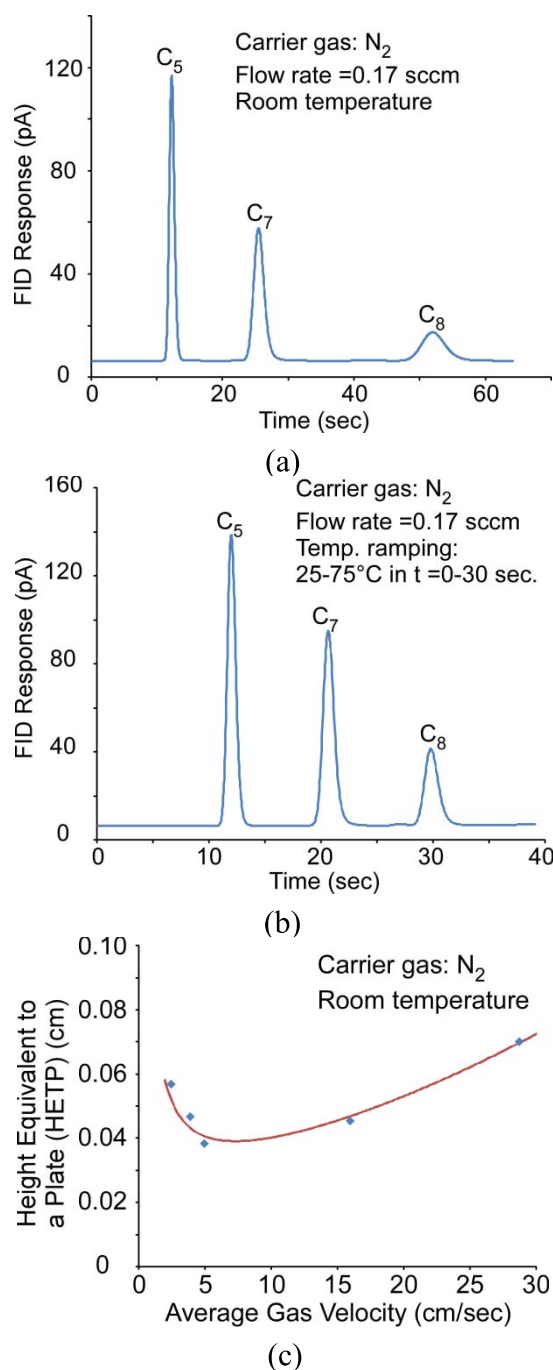


Fig. 8. The testing and evaluation results of the separation column. (a) The column separating a C<sub>5</sub>, C<sub>7</sub>, and C<sub>8</sub> alkane mixture at room temperature. (b) The column separating a C<sub>5</sub>, C<sub>7</sub>, and C<sub>8</sub> alkane mixture by linearly ramping the temperature from 25 °C to 75 °C in 30 sec. (c) The Golay plot of the separation column operating at room temperature; the evaluation is based on the C<sub>8</sub> peak.

to control the discharge current. The resistive dividers formed by R<sub>2</sub>/R<sub>3</sub> and R<sub>4</sub>/R<sub>5</sub> are connected to oscilloscope channels, so that the anode and cathode voltages as well as the discharge current can be observed.

The typical transient voltages observed at the anode and cathode are shown in Fig. 9(b). The anode took 1.6 ms to reach the breakdown voltage. The discharge current ran through the ballast resistor and raised the cathode voltage. Once initiated,

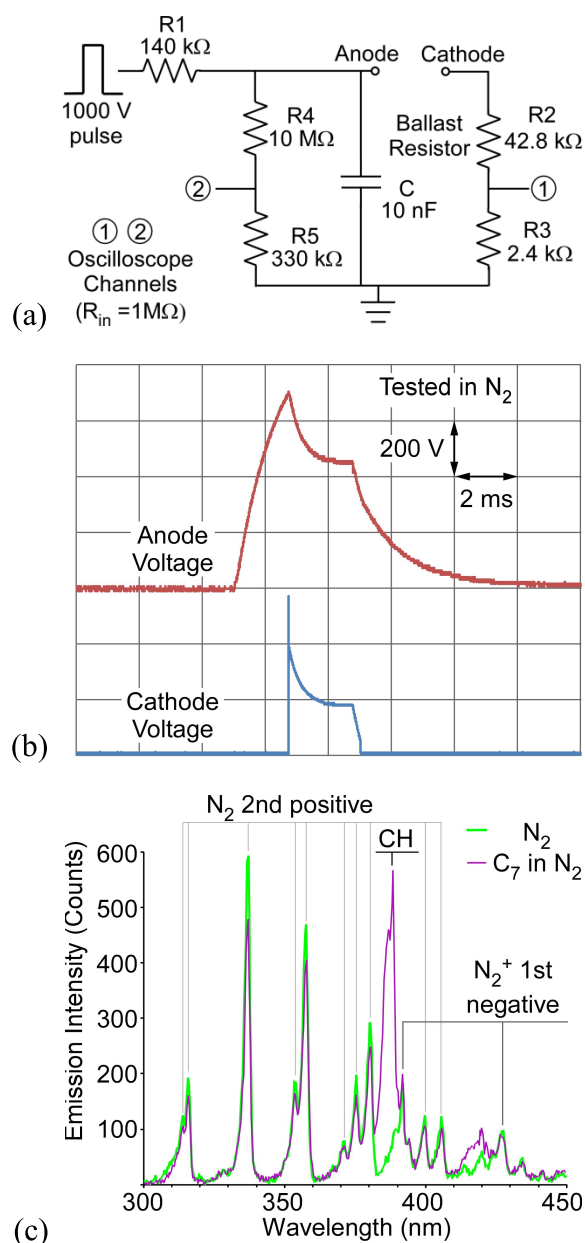


Fig. 9. The experimental testing and evaluation of the discharged-based detector. (a) The discharge circuitry. (b) The discharge waveform. (c) The optical spectrum generated by the discharge.

the discharge presented in the circuit as 73 kΩ resistance. The high voltage pulse lasted 3.5 ms, during which the actual discharge took 1.9 ms. During the pulse, the typical energy consumed by the discharge was 2.9 mJ, while the total energy consumed by the whole circuit was 13.3 mJ.

Optical emission from the microdischarge is guided by an optical fiber to a handheld spectrometer (Model # USB 2000, Ocean Optics, FL). The spectrometer uses a grating to diffract the incoming light. The resulting spatial distribution is captured by a charge-coupled device (CCD) array. The emission spectra, in the 300–450 nm window, of pure nitrogen and a heptane/nitrogen mixture are compared in Fig. 9(c). The emission associated with the N<sub>2</sub> second positive system contains lines at 314 nm, 316 nm, 337 nm, 353 nm, 357 nm, 371 nm, 375 nm, 380 nm, 399 nm and 405 nm, while that

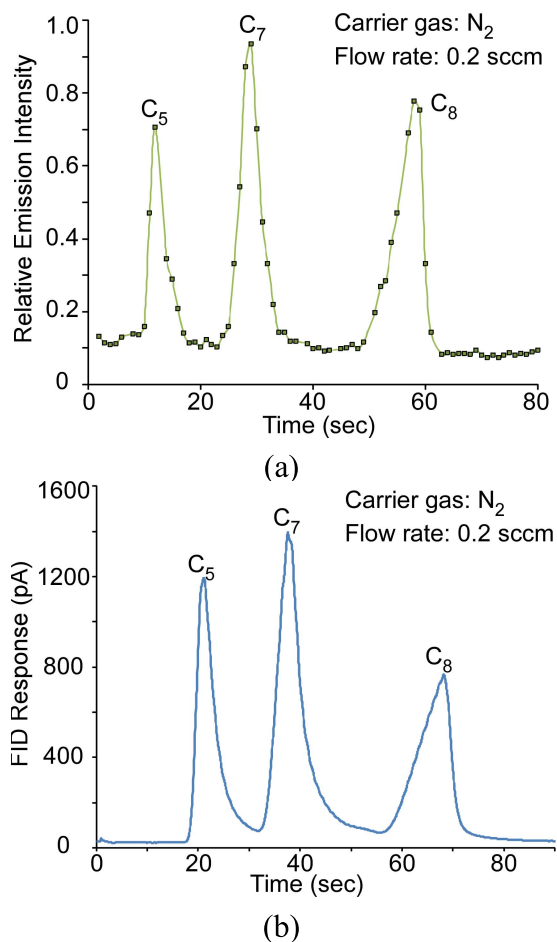


Fig. 10. The separation of pentane, heptane and octane by the fully stacked *iGC1* system. (a) The chromatogram provided by the discharge-based detector. (b) The corresponding chromatogram provided by the FID used as a reference.

associated with  $N_2^+$  first negative system contains lines at 391 nm and 426 nm [45]. With an elevated concentration of heptane, the emission spectrum shows a significant CH line at 387 nm [46]. The intensity ratio of the CH line at 387 nm to the  $N_2$  line at 337 nm was used as a measure of alkane strength to correct for possible variations in intensity from pulse to pulse. The data points with sufficient emission intensity (*i.e.*, greater than 50 counts at 337 nm line) were used to construct chromatograms.

#### E. The Stacked *iGC1* System

Typical chromatograms provided by the stacked *iGC1* system for alkane mixtures are shown in Fig. 10. Figure 10(a) shows the data collected by the discharge-based detector. The three peaks correspond to the separation and detection of pentane, heptane and octane. Figure 10(b) shows the benchmark FID response, verifying the results provides by the discharge-based detector. The FID signal lags behind that of the discharge-based detector as the FID is connected downstream of the *iGC1* stack. The relative peak heights among the three analytes are slightly different between the two chromatograms, possibly due to the emission characteristics of various species within the microdischarges. The power/energy

TABLE I  
POWER/ENERGY CONSUMPTION DURING THE *iGC1* SEPARATION

Component	Operation	Energy /Power	Comment
Knudsen pump	Steady state pumping	1.1 W	Steady state power
Preconcentrator	2 sec. thermal pulse	34 J	Desorption energy
Column	Temperature programming	1.06 W	Average power during ramping
Discharge-based detector	3.5 ms high voltage pulse	13.3 mJ/pulse	Energy per pulse
Stacked <i>iGC1</i> system	Separation without column programming	1.5 W	Average power during a run

TABLE II  
SUMMARY OF THE SYSTEM CHARACTERISTICS

<i>iGC1</i> volume	$\approx 3.7 \text{ cm}^3$
<i>iGC1</i> weight	$\approx 5$ grammes
Power	typically $\approx 1.5 \text{ W}$
Operation time	typically $\approx 6$ min.
External hardware	Heat sink
	Spectrometer
	Control electronics

consumption of the components and the *iGC1* system are summarized in Table I. The *iGC1* run as shown in Fig. 10 had an average power consumption of 1.5 W.

The results in Fig. 10(a) were obtained by first sampling a prepared vapor mixture. Driven by the integrated Knudsen pump, a mixture of pentane, heptane and octane in  $N_2$  was sampled into the preconcentrator for  $\approx 5$  min. When initiating the separation, the preconcentrator was heated to 170 °C in 2 sec. to inject the vapor analytes into the column. The Knudsen pump was supplied with 1.1 W power, providing a  $N_2$  flow rate of 0.2 sccm; the  $N_2$  carrier gas was supplied by a Tedlar bag connected upstream of the system. Temperature programming of the separation column was not used in this experiment. The detector was operated at 1 Hz (1 pulse/sec.) frequency. A customized LabVIEW® program was used to control the overall operation of the *iGC1* system.

#### V. DISCUSSION AND CONCLUSION

This work demonstrates the feasibility of using a standardized fabrication approach to manufacture a fluidic microsystem for gas chromatography, including a pump, a preconcentrator, a separation column and a detector. The fabrication process is low cost and standardized, showing promise of wider adoption of  $\mu\text{GC}$  technology. The assembly procedure described in this effort mainly focuses on die-to-die assembly after dicing. However, as noted earlier, wafer-to-wafer assembly prior to dicing can also be envisioned, enabling batch mode fabrication.

The 4-cm<sup>3</sup> *iGC1* system demonstrates that it is possible to mitigate thermal crosstalk between components to achieve a small form factor. The properties of the system are summarized in Table II. Discharge-based detectors are stable over time because the emission spectra are characteristics of the

chemical species present. The detection rate is mainly limited by the duration of plasma afterglow, which is typically less than 20 ms [22], corresponding to a detection rate of over 50 Hz. Nevertheless, the discharge-based detector requires special considerations because of background noise in an air ambient, and the need for high voltages. The miniaturization of spectrometers has previously been demonstrated [47], and versions as small as 19 cm<sup>3</sup> are commercially available (Model # Qstick, RGB Lasersysteme GmbH, Germany [48]), indicating the feasibility of a fully integrated system.

The use of epoxies in the system assembly provides a low-temperature (*i.e.*, less than 200 °C) and low-cost solution. The epoxies are chosen for low out-gassing properties and are sufficiently cured, minimizing the out-gassing problem. In preliminary studies, significant out-gassing was not observed, but the effects of higher temperatures remain unclear. As an alternative, spin-on-glass may be used for component assembly. It is expected not to contribute interferences to the chromatography, but its curing temperature is typically above 400 °C.

The effort of integrating a micro gas pump into the *iGCI* system provides a path for realizing a complete micro analytical system. The stackable architecture provides interchangeability, *i.e.*, different component designs can be readily fitted into the system, tailoring it for various applications. The analytical capability of the system can be extended to more complex gas environments by reconfiguring the system, such as direct stacking of more separation columns or even implementing a 2DGC system. Beyond the preliminary experimental results shown in this effort, more options of the *iGCI* operation are possible, such as the combination of temperature programming and flow programming (readily provided by the Knudsen pump [30]). Although the Knudsen pump utilized in this design does not provide optimal flow for the preconcentrator, future designs are expected to resolve this matter.

#### ACKNOWLEDGMENT

The authors thank Prof. Ken Wise and Robert Gordenker for providing access to test facilities, Dr. Seungdo An for wafer metallization, and Dr. Naveen Gupta, Dr. Jing Liu, Xin Luo, Prof. Katsuo Kurabayashi, and Prof. Xudong Fan for discussions.

#### REFERENCES

- [1] F. J. Santos and M. T. Galceran, "The application of gas chromatography to environmental analysis," *Trends Anal. Chem.*, vol. 21, nos. 9–10, pp. 672–685, 2002.
- [2] S. J. Lehotay and J. Hajšlová, "Application of gas chromatography in food analysis," *Trends Anal. Chem.*, vol. 21, nos. 9–10, pp. 686–697, 2002.
- [3] A. W. Boots, J. J. van Berkel, J. W. Dallinga, A. Smolinska, E. F. Wouters, and F. J. van Schooten, "The versatile use of exhaled volatile organic compounds in human health and disease," *J. Breath Res.*, vol. 6, no. 2, p. 027108, 2012.
- [4] S. C. Terry, J. H. Jerman, and J. B. Angell, "A gas chromatographic air analyzer fabricated on a silicon wafer," *IEEE Trans. Electron Devices*, vol. 26, no. 12, pp. 1880–1886, Dec. 1979.
- [5] A. Bhushan, D. Yemane, E. B. Overton, J. Goettert, and M. C. Murphy, "Fabrication and preliminary results for LiGA fabricated nickel micro gas chromatograph columns," *J. Microelectromech. Syst.*, vol. 16, no. 2, pp. 383–393, 2007.
- [6] M. Agah, J. A. Potkay, G. Lambertus, R. Sacks, and K. D. Wise, "High-performance temperature-programmed microfabricated gas chromatography columns," *J. Microelectromech. Syst.*, vol. 14, no. 5, pp. 1039–1050, 2005.
- [7] H. Noh, P. J. Hesketh, and G. C. Frye-Mason, "Parylene gas chromatographic column for rapid thermal cycling," *J. Microelectromech. Syst.*, vol. 11, no. 6, pp. 718–725, 2002.
- [8] J. A. Potkay, G. R. Lambertus, R. D. Sacks, and K. D. Wise, "A low-power pressure- and temperature-programmable micro gas chromatography column," *J. Microelectromech. Syst.*, vol. 16, no. 5, pp. 1071–1079, 2007.
- [9] S. Reidy, G. Lambertus, J. Reece, and R. Sacks, "High-performance, static-coated silicon microfabricated columns for gas chromatography," *Anal. Chem.*, vol. 78, no. 8, pp. 2623–2630, 2006.
- [10] G. Lambertus and R. Sacks, "Stop-flow programmable selectivity with a dual-column ensemble of microfabricated etched silicon columns and air as carrier gas," *Anal. Chem.*, vol. 77, no. 7, pp. 2078–2084, 2005.
- [11] M. A. Zareian-Jahromi and M. Agah, "Microfabricated gas chromatography columns with monolayer-protected gold stationary phases," *J. Microelectromech. Syst.*, vol. 19, no. 2, pp. 294–304, 2010.
- [12] W.-C. Tian, T. H. Wu, C.-J. Lu, W. R. Chen, and H. J. Sheen, "A novel micropreconcentrator employing a laminar flow patterned heater for micro gas chromatography," *J. Microelectromech. Syst.*, vol. 22, no. 6, pp. 065014-1–065014-8, 2012.
- [13] W.-C. Tian, H. K. L. Chan, C.-J. Lu, S. W. Pang, and E. T. Zellers, "Multiple-stage microfabricated preconcentrator-focuser for micro gas chromatography system," *J. Microelectromech. Syst.*, vol. 14, no. 3, pp. 498–507, 2005.
- [14] I. Voiculescu, M. Zaghloul, and N. Narasimhan, "Microfabricated chemical preconcentrators for gas-phase microanalytical detection systems," *Trends Anal. Chem.*, vol. 27, no. 4, pp. 327–343, 2008.
- [15] J. H. Seo, S. K. Kim, E. T. Zellers, and K. Kurabayashi, "Microfabricated passive vapor preconcentrator/injector designed for microscale gas chromatography," *Lab Chip*, vol. 12, no. 4, pp. 717–724, 2012.
- [16] K. Nachev, F. Marty, E. Donzier, B. Bourlon, K. Danaie, and T. Bourouina, "Micro gas chromatography sample injector for the analysis of natural gas," *J. Microelectromech. Syst.*, vol. 21, no. 3, pp. 730–738, 2012.
- [17] W. H. Steinecker, S. K. Kim, F. I. Bohrer, L. Farina, C. Kurdak, and E. T. Zellers, "Electron-beam patterned monolayer-protected gold nanoparticle interface layers on a chemiresistor vapor sensor array," *IEEE Sensors J.*, vol. 11, no. 2, pp. 469–480, Feb. 2011.
- [18] T. E. Mlsna, S. Cemalovic, M. Warburton, S. T. Hobson, D. A. Mlsna, and S. V. Patel, "Chemical capacitive microensors for chemical warfare agent and toxic industrial chemical detection," *Sens. Actuators B, Chem.*, vol. 116, nos. 1–2, pp. 192–201, 2006.
- [19] S. Narayanan, B. Alfeeli, and M. Agah, "Two-port static coated micro gas chromatography column with an embedded thermal conductivity detector," *IEEE Sensors J.*, vol. 12, no. 6, pp. 1893–1900, Jun. 2012.
- [20] K. Reddy, Y. Guo, J. Liu, W. Lee, M. K. K. Oo, and X. Fan, "Rapid, sensitive, and multiplexed on-chip optical sensors for micro-gas chromatography," *Lab Chip*, vol. 12, no. 5, pp. 901–905, 2012.
- [21] X. Luo, W. Zhu, B. Mitra, J. Liu, T. Liu, X. Fan, *et al.*, "A chemical detector for gas chromatography using pulsed discharge emission spectroscopy on a microchip," in *Proc. AGU Fall Meeting*, San Francisco, CA, USA, Dec. 2011, p. 0550.
- [22] B. Mitra and Y. B. Gianchandani, "The detection of chemical vapors in air using optical emission spectroscopy of pulsed microdischarges from two- and three- electrode microstructures," *IEEE Sensors J.*, vol. 8, no. 8, pp. 1445–1454, Aug. 2008.
- [23] S.-J. Kim, S. M. Reidy, B. P. Block, K. D. Wise, E. T. Zellers, and K. Kurabayashi, "Microfabricated thermal modulator for comprehensive two-dimensional micro gas chromatography: Design, thermal modeling, and preliminary testing," *Lab Chip*, vol. 10, no. 13, pp. 1647–1654, 2010.
- [24] G. Serrano, D. Paul, S.-J. Kim, K. Kurabayashi, and E. T. Zellers, "Comprehensive two-dimensional gas chromatographic separations with a microfabricated thermal modulator," *Anal. Chem.*, vol. 84, no. 16, pp. 6973–6980, 2012.
- [25] P. R. Lewis, R. P. Manginell, D. R. Adkins, R. J. Kottenstette, D. R. Wheeler, S. S. Sokolowski, *et al.*, "Recent advancements in the gas-phase MicroChemLab," *IEEE Sensors J.*, vol. 6, no. 3, pp. 784–795, Jun. 2006.

- [26] E. T. Zellers, G. Serrano, H. Chang, and L. K. Amos, "A micro gas chromatograph for high-speed determinations of explosive markers," in *Proc. IEEE Int. Conf. Solid-State Sens., Actuators Microsyst.*, Beijing, China, Jun. 2011, pp. 2082–2085.
- [27] S. K. Kim, H. Chang, and E. T. Zellers, "Prototype micro gas chromatograph for breath biomarkers of respiratory disease," in *Proc. IEEE Int. Conf. Solid-State Sens., Actuators Microsyst.*, Denver, CO, USA, Jun. 2009, pp. 128–131.
- [28] R. J. M. Gordenker and K. D. Wise, "A programmable palm-size gas analyzer for use in micro autonomous systems," *Proc. SPIE*, vol. 8373, pp. 83731O-1–83731O-6, Apr. 2012.
- [29] H. Kim, W. H. Steinecker, S. Reidy, G. R. Lambertus, A. A. Astle, K. Najafi, *et al.*, "A micropump-driven high-speed MEMS gas chromatography system," in *Proc. IEEE Int. Conf. Solid-State Sens., Actuators Microsyst. Conf.*, Lyon, France, Jun. 2007, pp. 1505–1508.
- [30] J. Liu, N. K. Gupta, K. D. Wise, Y. B. Gianchandani, and X. Fan, "Demonstration of motionless Knudsen pump based micro-gas chromatography featuring micro-fabricated columns and on-column detectors," *Lab Chip*, vol. 11, no. 20, pp. 3487–3492, 2011.
- [31] N. K. Gupta and Y. B. Gianchandani, "Thermal transpiration in mixed cellulose ester membranes: Enabling miniature, motionless gas pumps," *Microporous Mesoporous Mater.*, vol. 142, nos. 2–3, pp. 535–541, 2011.
- [32] H. van Weerden, G.-J. Burger, and J. Elders, "Fast micro-GC capabilities based on a microintegration technology platform," *Amer. Lab.*, vol. 40, no. 16, pp. 14–15, 2008.
- [33] R. P. Manginell, D. R. Adkins, M. W. Moorman, R. Hadizadeh, D. Copic, D. A. Porter, *et al.*, "Mass-sensitive microfabricated chemical preconcentrator," *J. Microelectromech. Syst.*, vol. 17, no. 6, pp. 1396–1407, 2008.
- [34] D. R. Adkins, "Modular manifold for integrated fluidics and electronics," U.S. Patent 7685864, Mar. 30, 2010.
- [35] D. R. Adkins and P. R. Lewis, "Compact low-power gas detector for chemical alarms," *Proc. SPIE*, vol. 7304, pp. 73040S-1–73040S-10, Apr. 2009.
- [36] P. R. Lewis and D. R. Wheeler, "Non-planar microfabricated gas chromatography column," U.S. Patent 7273517, Sep. 25, 2007.
- [37] R. P. Manginell, J. M. Bauer, M. W. Moorman, L. J. Sanchez, J. M. Anderson, J. J. Whiting, *et al.*, "A monolithically-integrated  $\mu$ GC chemical sensor system," *Sensors*, vol. 11, no. 7, pp. 6517–6532, 2011.
- [38] Y. Qin and Y. B. Gianchandani, "A facile, standardized fabrication approach and scalable architecture for a micro gas chromatography system with integrated pump," in *Proc. IEEE Int. Conf. Solid-State Sens., Actuators Microsyst.*, Barcelona, Spain, Jun. 2013, pp. 2755–2758.
- [39] F. Sharipov, "Rarefied gas flow through a long tube at any temperature ratio," *J. Vac. Sci. Technol. A, Vac. Surf. Films*, vol. 14, no. 4, pp. 2627–2635, 1996.
- [40] L. A. Jonas and J. A. Rehrmann, "Predictive equations in gas adsorption kinetics," *Carbon*, vol. 11, no. 1, pp. 59–64, 1973.
- [41] P. Lodewyckx, G. O. Wood, and S. K. Ryu, "The Wheeler–Jonas equation: A versatile tool for the prediction of carbon bed breakthrough times," in *Proc. Carbon Conf.*, Oviedo, Spain, Jul. 2003, pp. 1345–1349.
- [42] E. F. Barry, "Columns: Packed and capillary; column selection in gas chromatography," in *Modern Practice of Gas Chromatography*, R. L. Grob and E. F. Barry, Eds. Hoboken, NJ, USA: Wiley, 2004, pp. 65–191.
- [43] C. K. Eun and Y. B. Gianchandani, "Microdischarge-based sensors and actuators for portable microsystems: Selected examples," *IEEE J. Quantum Electron.*, vol. 48, no. 6, pp. 814–826, Jun. 2012.
- [44] B. Mitra, B. Levey, and Y. B. Gianchandani, "Hybrid arc/glow microdischarges at atmospheric pressure and their use in portable systems for liquid and gas sensing," *IEEE Trans. Plasma Sci.*, vol. 36, no. 4, pp. 1913–1924, Aug. 2008.
- [45] R. R. O'Neil and G. Davidson, "The fluorescence of air and nitrogen excited by energetic electrons," Tech. Rep. 12, Amer. Sci. Eng. Inc., Cambridge, MA, USA, Jan. 1968.
- [46] R. W. Pearse and A. G. Gaydon, *The Identification of Molecular Spectra*. London, U.K.: Chapman & Hall, 1950.
- [47] L. Que, C. G. Wilson, and Y. B. Gianchandani, "Microfluidic electrodischarge devices with integrated dispersion optics for spectral analysis of water impurities," *J. Microelectromech. Syst.*, vol. 14, no. 2, pp. 185–191, 2005.
- [48] RGB Lasersysteme GmbH, Toledo, OH, USA. (2014, Feb. 19). *Qstick—The World's First USB Stick Spectrometer* [Online]. Available: [http://www.rgb-laser.com/content\\_products/product\\_qstick.html](http://www.rgb-laser.com/content_products/product_qstick.html)



**Yutao Qin** received the B.S.E. degree in electronic science and technology (microelectronics) from South China University of Technology, Guangzhou, China, in 2010 and the M.S.E. degree in electrical engineering from the University of Michigan, Ann Arbor, MI, USA, in 2012. He is currently pursuing the Ph.D. degree in electrical engineering at the University of Michigan, Ann Arbor. His research interests include micro gas chromatography systems and Knudsen pumps.



**Yogesh B. Gianchandani** (M'86–SM'05–F'10) is a Professor at the University of Michigan, Ann Arbor, with a primary appointment in the Electrical Engineering and Computer Science Department and a courtesy appointment in the Mechanical Engineering Department. He also serves as the Director for the Center for Wireless Integrated MicroSensing and Systems (WIMS<sup>2</sup>). Dr. Gianchandani's research interests include all aspects of design, fabrication, and packaging of micromachined sensors and actuators (<http://www.eecs.umich.edu/~yogesh/>). He has published about 300 papers in journals and conferences, and has about 35 US patents issued or pending. He was a Chief Co-Editor of *Comprehensive Microsystems: Fundamentals, Technology, and Applications*, published in 2008. From 2007 to 2009 he also served at the National Science Foundation, as the program director for Micro and Nano Systems within the Electrical, Communication, and Cyber Systems Division (ECCS).